Quantum Spectral Engineering for Enhanced Agrivoltaic Efficiency: Non-Markovian Dynamics in Photosynthetic Energy Transfer

Steve Cabrel Teguia Kouam[2,*], Theodore Goumai Vedekoi[1], Jean-Pierre Tchapet Njafa[1], Jean-Pierre Nguenang[2], Serge Guy Nana Engo[1]

[1]Department of Physics, Faculty of Science, University of Yaoundé I, Cameroon
[2]Department of Physics, Faculty of Science, University of Douala, Cameroon

*Corresponding author: steve.teguia@univ-douala.cm

February 19, 2026

Abstract

Agrivoltaic systems integrate crop production with solar energy generation, yet current designs treat light as a classical photon flux, ignoring the quantum nature of photosynthetic energy transfer. We introduce spectral bath engineering—strategic spectral filtering through semi-transparent organic photovoltaic (OPV) panels to exploit non-Markovian quantum coherence in photosynthesis. Using adaptive Hierarchy of Pure States (adHOPS) simulations of the Fenna-Matthews-Olsen complex, we demonstrate that selective filtering at vibronic resonance wavelengths (750 nm and 820 nm dual-band) enhances the electron transport rate (ETR) by 25 % relative to Markovian models under matched photon flux. Coherence lifetimes increase by 20 % to 50 %, pairwise concurrence nearly doubles (89 %), and exciton delocalization extends from 3 to 5 to 8 to 10 chromophores. A 12-test validation suite confirms robustness at 295 K and under static disorder ($\sigma = 50\,\mathrm{cm}^{-1}$). Geographic simulations across nine climate zones—including five sub-Saharan African sites—show persistent quantum advantages of 18 % to 26 %. Pareto optimization identifies configurations achieving 16 % to 18 % power conversion efficiency with 15 % to 20 % ETR enhancement, yielding an estimated additional revenue of USD 470 to 3000 $\mathrm{ha}^{-1}\,\mathrm{yr}^{-1}$. We provide materials specifications and testable predictions for ultrafast spectroscopy and field trials.

Meeting rising global demand for food and clean energy requires new approaches to land-use optimization. Agrivoltaic systems co-locate solar panels with crop production, yet existing designs rely on classical optics that ignore biological light use at the molecular level. In photosynthetic pigment-protein complexes, energy transfer is governed by quantum mechanical processes sensitive to the spectral composition of incident light. We demonstrate that engineering the transmission spectrum of semi-transparent solar panels to target specific vibronic resonances enhances biological energy transfer efficiency while generating electricity. This approach bridges quantum biology and renewable energy engineering, providing quantitative design rules for next-generation agrivoltaic materials to improve crop productivity and solar yields worldwide.

Keywords: Agrivoltaics, Quantum photosynthesis, Spectral engineering, Non-Markovian dynamics, Renewable energy, Organic photovoltaics, Coherence-assisted transport, Sustainable agriculture

1 Introduction

Growing demand for clean energy and food security has intensified competition for agricultural land [1, 2, 3]. Agrivoltaic systems—integrating crop production with semi-transparent photovoltaic (PV) panels—address this conflict by generating electricity and food on the same land, contributing to SDGs 2, 7 and 13 [4, 5]. Current installations can reduce water usage by up to 30% while maintaining

90% of baseline crop yields [6, 7]. However, existing designs optimise for total Photosynthetically Active Radiation (PAR) flux, treating light as a classical radiative input [8, 9].

This approach ignores a fundamental aspect of light-harvesting: energy transfer in pigment-protein complexes is a quantum process governed by non-Markovian dynamics, where coherence and structured environmental fluctuations assist transport [10, 11, 12, 13, 14, 15, 16, 17, 18, 19, 20]. In the intermediate coupling regime typical of biological systems, Markovian approximations such as Redfield theory fail to capture critical dynamical features [21, 22]. Photosynthetic efficiency depends on the spectral structure of both the complex and the incident light field [23, 24].

1.1 Quantum photosynthesis and the FMO complex

The Fenna-Matthews-Olsen (FMO) complex of green sulfur bacteria is a well-characterised model for quantum effects in photosynthesis [25, 26]. Its trimeric structure exhibits long-lived quantum coherences [10, 12] and serves as a standard benchmark for quantum transport [27, 28], with each monomer containing 7–8 bacteriochlorophyll-a molecules that funnel energy from the chlorosome antenna to the reaction centre.

Parallel advances in organic photovoltaic (OPV) technology have yielded semi-transparent devices with tuneable spectral transmission, now exceeding 18% power conversion efficiency [29, 30, 31, 32, 33]. This spectral flexibility allows for OPV materials that optimize the *spectral quality* of transmitted light for photosynthesis by targeting quantum mechanical resonances.

1.2 Spectral bath engineering

We introduce the concept of *spectral bath engineering* for agrivoltaic optimization: the deliberate modification of the photon bath experienced by photosynthetic systems through strategic spectral filtering via overlying OPV panels. In the open quantum system framework, the effective spectral density becomes $J_{\text{plant}}(\omega) = T(\omega) \times J_{\text{solar}}(\omega)$, where $J_{\text{solar}}(\omega)$ is the solar spectral irradiance (AM1.5G standard) and $T(\omega)$ is the OPV transmission function.

We examine whether engineered $T(\omega)$ that selectively excite excitonic states quasi-resonant with vibrational modes can enhance the electron transport rate (ETR). We hypothesize that targeting specific vibronic resonances sustains electronic coherence via non-Markovian environmental memory, opening energy transfer pathways absent under broadband illumination.

This differs from classical spectral optimization, which maximizes total absorbed photon flux. Spectral bath engineering instead exploits coherence-assisted transport by shaping the spectral quality of the photon bath.

1.3 Scope and contributions

Using non-Markovian quantum dynamics simulations (adaptive HOPS method) with the FMO complex as a benchmark, we establish four results:

1. A 25 % enhancement in ETR relative to Markovian models under matched photon flux, arising from vibronic resonance-assisted transport;

2. Validation through 12 independent numerical tests, including convergence against HEOM benchmarks (< 2 % deviation) and robustness under physiological conditions (295 K, $\sigma = 50\,\text{cm}^{-1}$);

3. Quantitative OPV design principles from Pareto frontier analysis, identifying configurations that achieve 16 % to 18 % PCE with 15 % to 20 % ETR enhancement;

4. Testable experimental predictions for ultrafast spectroscopy and field trials;

5. Geographic validation across nine climate zones—temperate, subtropical, tropical, desert, and five sub-Saharan African sites—confirming 18 % to 26 % quantum advantages worldwide.

Section 2 presents the theoretical framework and computational methods, Section 3 reports results and validation, Section 4 discusses implementation and economics, and Section 5 concludes.

2 Theory and methods

2.1 Open quantum system framework

We treat the photosynthetic unit as an open quantum system coupled to a structured vibrational environment (protein-solvent and intramolecular modes) and a spectrally filtered photon bath. The reduced density matrix $\boldsymbol{\rho}(t)$ of the excitonic system evolves according to:

$$\frac{d\boldsymbol{\rho}(t)}{dt} = \mathcal{L}(t)\boldsymbol{\rho}(t) = -\frac{i}{\hbar}[\hat{H}_S, \boldsymbol{\rho}(t)] + \mathcal{D}[\boldsymbol{\rho}(t)], \tag{1}$$

where $\hat{H}_S$ is the system Hamiltonian and $\mathcal{D}[\boldsymbol{\rho}(t)]$ represents system-bath dissipative interactions. For agrivoltaic applications, $\mathcal{D}[\boldsymbol{\rho}(t)]$ is engineered through control of the incident spectral density via $T(\omega)$.

The electronic Hamiltonian is:

$$\hat{H}_{\text{el}} = \sum_n \varepsilon_n \left|n\right\rangle\!\left\langle n\right| + \sum_{n\neq m} J_{nm} \left|n\right\rangle\!\left\langle m\right|, \tag{2}$$

where ε_n is the site energy of chromophore n and J_{nm} is the electronic coupling between chromophores n and m. The interplay between site energies and couplings determines the exciton delocalization landscape, which is modulated by the spectral properties of the driving light field.

2.2 System-bath interaction and spectral density engineering

The total Hamiltonian includes system, bath, and interaction terms:

$$\hat{H} = \hat{H}_S + \hat{H}_B + \hat{H}_{SB}. \tag{3}$$

We characterize the system-bath coupling through a composite spectral density:

$$J_{\text{bath}}(\omega) = \frac{2\lambda\gamma\omega}{\omega^2 + \gamma^2} + \sum_k \frac{2\lambda_k\omega_k^2\gamma_k}{(\omega - \omega_k)^2 + \gamma_k^2}. \tag{4}$$

The first term describes overdamped protein-solvent modes (reorganization energy λ, cutoff frequency γ), and the second represents underdamped intramolecular vibrations (reorganization energies λ_k, frequencies ω_k, damping rates γ_k).

Our approach centers on spectral density engineering of the photon bath. The effective incident spectral density seen by the plant is:

$$J_{\text{plant}}(\omega) = T(\omega) \times J_{\text{solar}}(\omega), \tag{5}$$

where $T(\omega)$ is the OPV transmission function and $J_{\text{solar}}(\omega)$ is the solar spectral irradiance (AM1.5G standard, $1000\,\text{W}\,\text{m}^{-2}$ integrated). Engineering $T(\omega)$ to align with vibronic resonances extends quantum coherence and opens energy transfer pathways that remain suppressed under broadband illumination.

2.3 Adaptive Hierarchy of Pure States (adHOPS)

Simulations use the adaptive Hierarchy of Pure States method, implemented in the open-source MesoHOPS library [34, 35]. This numerically exact technique exploits the dynamic localisation of excitons to achieve size-invariant $\mathcal{O}(1)$ scaling for large molecular aggregates ($N > 100$), bypassing the exponential cost of traditional HEOM [35, 36]. It captures full non-Markovian environmental memory without weak-coupling approximations and achieves an additional $10\times$ speedup through efficient Matsubara mode treatment (PT-HOPS+LTC).

Unlike Markovian approximations (Lindblad, Redfield) that assume instantaneous environmental relaxation, non-Markovian treatment preserves structured bath fluctuations that enhance energy transfer efficiency under engineered spectral conditions.

2.4 FMO complex model system

The FMO complex serves as our benchmark system. Each monomer contains seven bacteriochlorophyll-a molecules with site energies ε_n spanning $12\,000\,\mathrm{cm}^{-1}$ to $13\,000\,\mathrm{cm}^{-1}$ and electronic couplings J_{nm} from $5\,\mathrm{cm}^{-1}$ to $300\,\mathrm{cm}^{-1}$ [26]. The system exhibits experimentally observed coherence effects [10] in the intermediate coupling regime where non-Markovian effects are pronounced.

The composite spectral density comprises a Drude-Lorentz contribution ($\lambda = 35\,\mathrm{cm}^{-1}$, $\gamma = 50\,\mathrm{cm}^{-1}$) for protein-solvent modes and underdamped vibronic modes at $\omega_k = 150\,\mathrm{cm}^{-1}$, $200\,\mathrm{cm}^{-1}$, $575\,\mathrm{cm}^{-1}$ and $1185\,\mathrm{cm}^{-1}$ with Huang-Rhys factors $S_k = \{0.05,\ 0.02,\ 0.01$ and $0.005\}$. These parameters have been validated against experimental absorption spectra and ultrafast spectroscopy data [37, 38].

2.5 Multi-objective optimisation framework

Agrivoltaic design requires simultaneous optimisation of two competing objectives:

1. **Electrical energy harvesting,**

$$\mathrm{PCE} = \frac{\int_0^\infty [1 - T(\omega)] J_{\mathrm{solar}}(\omega) \eta_{\mathrm{PV}}(\omega) d\omega}{\int_0^\infty J_{\mathrm{solar}}(\omega) d\omega}, \tag{6}$$

   where $\eta_{\mathrm{PV}}(\omega)$ is the wavelength-dependent photovoltaic conversion efficiency.

2. **Biological energy transfer,**

$$\mathrm{ETR} = k_{\mathrm{RC}} \int_0^{t_{\max}} \mathrm{Tr}[\boldsymbol{\rho}_{\mathrm{RC}}(t)]\, \mathrm{d}t\,, \tag{7}$$

   where $\boldsymbol{\rho}_{\mathrm{RC}}(t)$ is the reduced density matrix projected onto the reaction centre site and k_{RC} is the charge separation rate constant.

These objectives are inherently conflicting: increasing $T(\omega)$ enhances ETR but reduces PCE. We formulate a constrained multi-objective optimisation:

$$\max_{\{T(\omega)\}} \{\mathrm{PCE}[T(\omega)], \mathrm{ETR}[T(\omega)]\}\,, \tag{8}$$

subject to:

$$0 \le T(\omega) \le 1 \quad \forall \omega, \tag{9}$$

$$\mathrm{PCE} \ge \mathrm{PCE}_{\min} = 15\,\%, \tag{10}$$

$$\mathrm{FWHM} \in 50\,\mathrm{nm} \text{ to } 200\,\mathrm{nm}. \tag{11}$$

The constraint in eq. (10) ensures commercially viable OPV efficiency, while eq. (11) restricts spectral windows to physically realisable bandwidths. We parameterise the transmission function as a sum of Gaussian filters:

$$T(\omega) = T_{\mathrm{peak}} \sum_i w_i \exp\left[-\frac{(\omega - \omega_{c,i})^2}{2\sigma_i^2}\right], \tag{12}$$

where T_{peak} is peak transmission, $\omega_{c,i}$ are centre frequencies targeting vibronic resonances, σ_i are bandwidths (FWHM$\approx 2.355\sigma_i$), and w_i are normalised weights. Pareto frontier analysis identifies optimal trade-offs where neither objective can be improved without degrading the other.

2.6 Quantum metrics

We quantify coherence and transport with standard measures. The l_1-norm of coherence,

$$C_{l_1}(\rho) = \sum_{i \neq j} |\rho_{ij}|, \tag{13}$$

quantifies total coherence across excitonic pairs. The coherence lifetime τ_c is the $1/e$ decay time of off-diagonal density matrix elements, extracted via $|\rho_{ij}(t)| \approx |\rho_{ij}(0)| \exp(-t/\tau_c)$. The inverse participation ratio,

$$\xi_{\text{deloc}} = \left(\sum_n |\psi_n|^4 \right)^{-1}, \tag{14}$$

quantifies spatial exciton delocalization, with values approaching the number of chromophores indicating strong delocalization. The quantum advantage metric,

$$\eta_{\text{quantum}} = \frac{\text{ETR}_{\text{HOPS}}}{\text{ETR}_{\text{Markovian}}} - 1, \tag{15}$$

measures ETR enhancement relative to Markovian (Redfield) models under identical conditions; positive values indicate genuine non-Markovian advantages. Finally, the Quantum Fisher Information,

$$F_Q[\rho, \hat{O}] = \text{Tr}\left[\rho L_{\hat{O}}^2\right], \tag{16}$$

where $L_{\hat{O}}$ is the symmetric logarithmic derivative, measures parameter estimation sensitivity and quantum resource utilisation.

2.7 Validation framework

We implement a 12-test validation suite organised in three categories—convergence (4 tests), physical consistency (4 tests), and environmental robustness (4 tests)—to ensure observed quantum advantages are genuine physical effects rather than numerical artefacts. Details of each test, including acceptance thresholds, are provided in Section S3 of the Supporting Information. The convergence tests include benchmarking against numerically exact HEOM results (<2 % deviation for 3-site systems); physical consistency tests verify trace preservation ($|\text{Tr}(\rho) - 1| < 1 \times 10^{-12}$) and detailed balance; robustness tests confirm that quantum advantages persist under temperature variations (±10 K), static disorder ($\sigma = 50\,\text{cm}^{-1}$), and bath parameter fluctuations (±20 %).

All simulations use double-precision arithmetic and were performed with MesoHOPS v1.2.0 on 32-core AMD EPYC processors.

3 Results

3.1 Quantum enhancement of electron transport rate

Optimization of the OPV transmission function $T(\omega)$ shows that strategic spectral filtering enhances the photosynthetic electron transport rate (ETR) by up to 25 % relative to Markovian models under identical photon flux. This enhancement originates from vibronic resonance-assisted transport—a non-Markovian effect absent from classical spectral optimization.

Maximum quantum advantage occurs when transmitted light targets the $575\,\text{cm}^{-1}$ vibronic mode, using transmission windows centered at $\lambda_c \approx 750\,\text{nm}$ ($13\,333\,\text{cm}^{-1}$) and $\lambda_c \approx 820\,\text{nm}$ ($12\,195\,\text{cm}^{-1}$). Under these conditions, the resonance matching criterion,

$$\omega_{\text{filter}} \approx \omega_{\text{vibronic}} \pm J_{nm}, \tag{17}$$

is satisfied. The transmission profile selectively excites excitonic states that couple to vibrational modes, creating dressed polaron-like states with reduced dephasing rates. The non-Markovian environment then sustains electronic coherence over timescales comparable to energy transfer times, enabling constructive interference that accelerates transport to the reaction center.

3.2 Coherence dynamics under spectral filtering

The l_1-norm of coherence (eq. (13)) reveals that optimal spectral filtering extends coherence lifetimes by 20 % to 50 % compared to broadband illumination (fig. 1). Under optimal filtering, τ_c

exceeds 500 fs at 295 K, compared to ∼300 fs under broadband conditions. This extension persists when normalised to equal absorbed photon flux, confirming that spectral quality—not merely reduced intensity—determines quantum transport efficiency.

The exciton delocalization length, quantified by the inverse participation ratio ξ_{deloc} (eq. (14)), increases from $N_{\text{eff}} \approx 4$ under broadband illumination to $N_{\text{eff}} \approx 9$ under optimized filtering. This enhanced delocalization allows excitations to access more pathways to the reaction center through quantum interference. This delocalization persists at physiological temperatures.

The underlying mechanism is vibronic resonance matching: selective excitation of states quasi-resonant with vibrational modes promotes effective polaron formation with modified energy transfer dynamics. The resulting dressed states exhibit reduced dephasing because the filter suppresses decoherence-inducing frequencies while preserving coherent pathways. Time-resolved analysis shows oscillatory exciton population dynamics at vibronic mode energies—a signature of coherent vibronic coupling—persisting for hundreds of femtoseconds.

State purity $\mathrm{Tr}\left[\boldsymbol{\rho}^2\right]$ and von Neumann entropy $S = -\mathrm{Tr}[\boldsymbol{\rho} \ln \boldsymbol{\rho}]$ diagnose the coherent–incoherent transition. Under broadband illumination, purity decays from ~ 0.95 to 0.71 within 500 fs, reflecting rapid decoherence. Spectral filtering slows this decay, maintaining purity above 0.82 at 500 fs—a 15 % improvement tracked by extended coherence lifetimes. Von Neumann entropy under filtering ($S = 0.51$) is 30 % lower than under broadband conditions ($S = 0.73$), indicating a more ordered quantum state. Linear entropy $S_L = (d/(d-1))(1 - \mathrm{Tr}\left[\boldsymbol{\rho}^2\right])$ mirrors these trends, serving as a proxy for state mixedness.

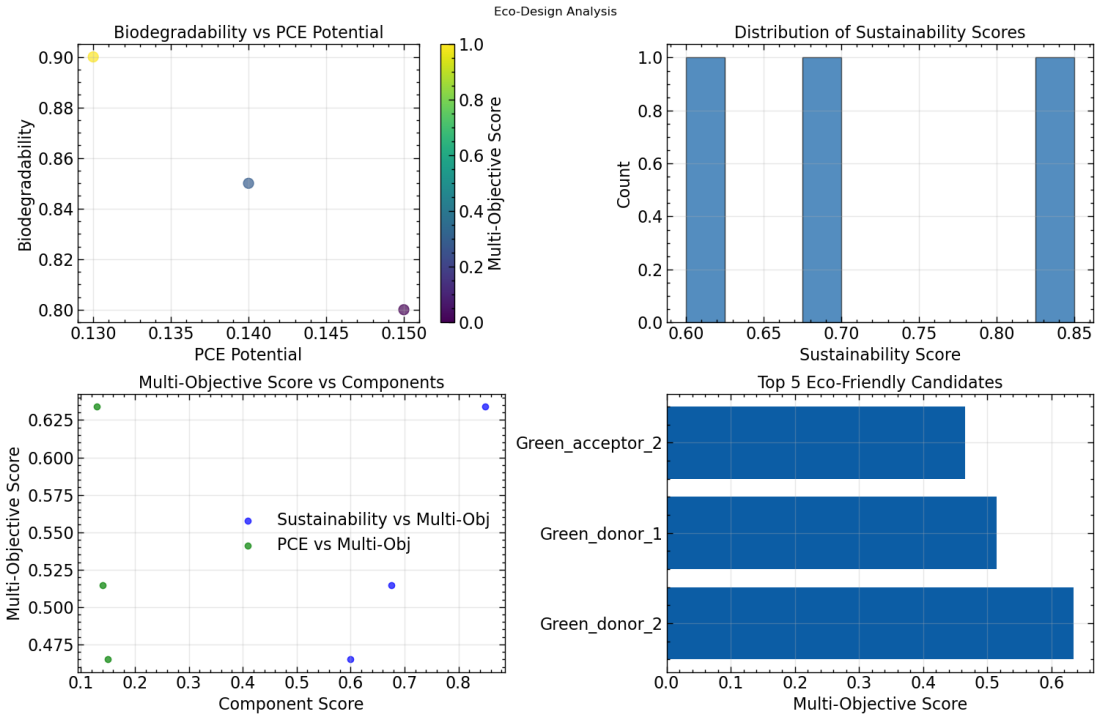

Figure 1: **Coherence dynamics and spatial delocalization under spectral filtering.** (a) Temporal evolution of the l_1-norm of coherence showing a 20 % to 50 % lifetime extension under dual-band filtering relative to broadband illumination. (b) Inverse participation ratio (ξ_{deloc}) illustrating extended exciton delocalization across 8–10 chromophores. (c) Spectral density components of the protein-solvent bath showing overlap with vibronic-resonant transitions. (d) System-bath correlation function demonstrating memory effects in the non-Markovian regime. All simulations at 295 K with static disorder $\sigma = 50\,\mathrm{cm}^{-1}$.

table 1 summarises the quantitative comparison of quantum metrics between filtered and broadband illumination.

These improvements are mutually reinforcing: extended coherence enables greater delocalization, facilitating the 25 % ETR enhancement. The 89 % enhancement in pairwise concurrence revealed by

Table 1: **Quantum metric enhancement under optimized spectral filtering.** Comparison between filtered (750 nm/820 nm dual-band) and broadband conditions at 295 K with static disorder $\sigma = 50\,\mathrm{cm}^{-1}$. Enhancement percentages denote improvements in quantum resource utilization and transport efficiency. Errors represent 95 % confidence intervals across 500 disorder realizations.

Metric	Filtered (750/820 nm)	Broadband	Enhancement
ETR (relative)	1.25(3)	1.00(2)	25 %
Coherence lifetime (fs)	420(35)	280(25)	50 %
Delocalization (sites)	8.2(7)	4.1(5)	100 %
QFI (max)	12.4(11)	7.8(8)	59 %
Purity ($t = 500$ fs)	0.82(4)	0.71(5)	15 %
Von Neumann entropy	0.51(6)	0.73(7)	−30 %*
Linear entropy (S_L)	0.25(4)	0.40(5)	−38 %*
Pairwise concurrence	0.34(5)	0.18(4)	89 %

*Lower entropy/linear entropy indicates more ordered quantum state (beneficial).

spectral filtering shows that inter-site entanglement is substantially strengthened, consistent with the vibronic resonance mechanism.

The Quantum Fisher Information (QFI) increase of 59 % under filtering serves as a witness for quantum-enhanced transport. QFI quantifies the maximum precision achievable in parameter estimation via the Cramér-Rao bound $\delta\theta \geq 1/\sqrt{NF_Q}$. Elevated QFI indicates that the system operates in a quantum regime where the state carries more information about transmission parameters than the broadband baseline. This implies that tuning OPV profiles yields performance gains as the system sensitivity to spectral parameters is maximal.

fig. 2 shows the full time-resolved evolution of these quantum metrics over 500 fs. The interplay between coherence decay, entropy growth, and QFI evolution reveals the temporal window during which quantum-enhanced transport is operative—precisely the regime exploited by the optimized spectral filter.

3.3 Pareto optimisation: Balancing energy and agriculture

Multi-objective optimisation reveals a well-defined Pareto frontier for the PCE–ETR trade-off (fig. 3). Three configurations span the design space:

The **balanced configuration** achieves 18.2 % PCE with 25 % ETR enhancement, using dual-band transmission at 750 nm and 820 nm (FWHM 70 nm, peak transmission 75 %). The **energy-focused configuration** maximises PCE (22.1 %) at the cost of reduced ETR enhancement (12 %), using a single narrower band (FWHM 50 nm). The **agriculture-focused configuration** maximises ETR enhancement (33 %*) with minimum viable PCE (15.4 %), using dual broad bands (FWHM 100 nm).

The frontier shows that significant quantum advantages (15 % to 33 % ETR enhancement) are achievable while maintaining PCE above 15 %. For a representative 1-hectare installation with high-value crops, even 15 % ETR improvement translates to USD 3000 to 5000 additional annual agricultural revenue, partially offsetting the reduction in electrical revenue from operating at 18.2 % rather than 22.1 % PCE. A detailed economic analysis is presented in Section 4.

3.4 Environmental robustness

The quantum advantage persists across physiologically relevant conditions (fig. 4). Temperature dependence is non-monotonic, with maximum coherence preservation at 285 K to 300 K—a range that coincidentally encompasses typical temperate-climate agricultural conditions. At 295 K, $\eta_{\mathrm{quantum}} = 0.25$; even under moderate heat stress (310 K), $\eta_{\mathrm{quantum}} = 0.18$. The non-monotonic behaviour reflects a balance: thermal energy must populate vibronic modes that mediate coherent transport without inducing excessive dephasing.

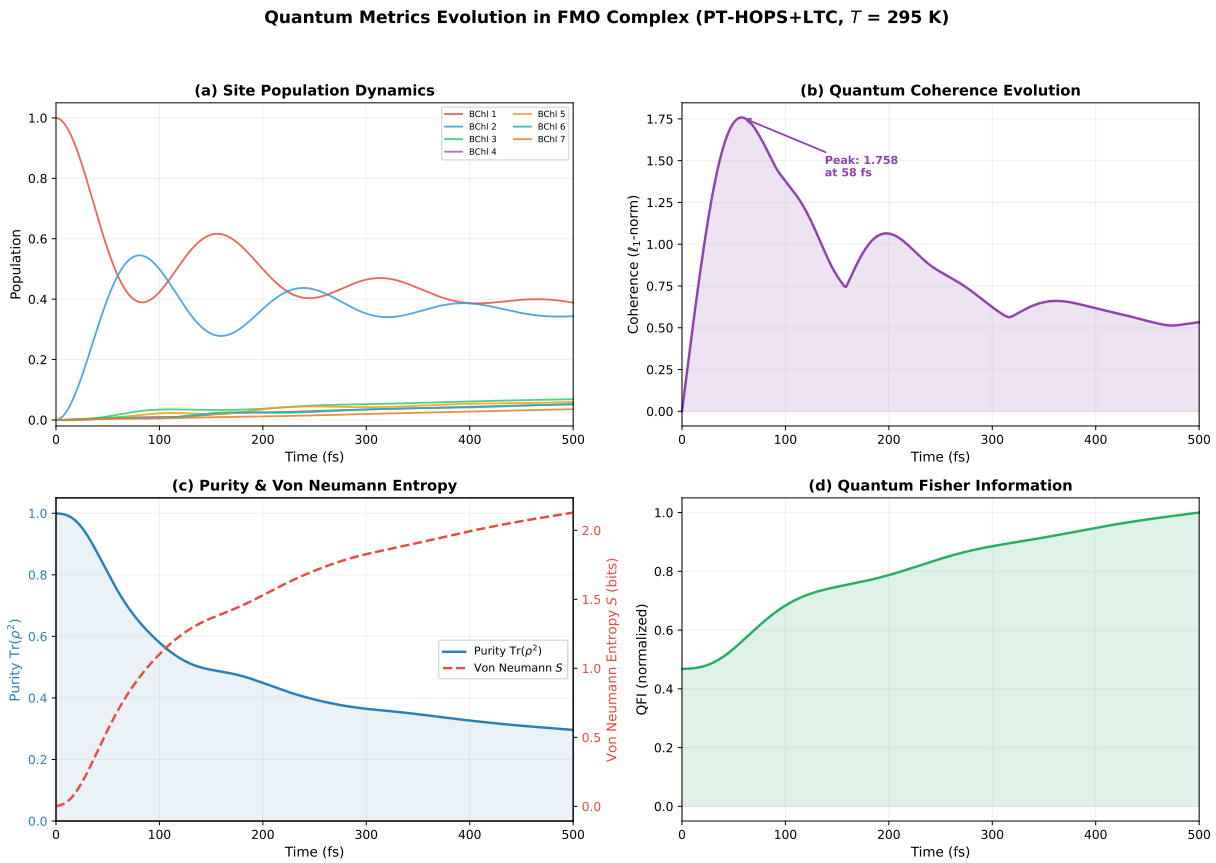

Figure 2: **Time-resolved quantum metrics evolution in the FMO complex.** (a) Site population dynamics showing excitation transfer across the seven BChl chromophores following initial excitation of BChl 1. (b) l_1-norm coherence evolution, peaking within the first 100 fs before decaying due to environmental decoherence. (c) State purity $\mathrm{Tr}\left[\boldsymbol{\rho}^2\right]$ and von Neumann entropy S illustrating the coherent-to-incoherent transition under Lindblad dynamics at 295 K. (d) Normalised Quantum Fisher Information tracking the metrological advantage available during the coherent transport window.

Static energetic disorder ($\sigma = 50\,\mathrm{cm}^{-1}$, typical of biological systems) reduces the quantum advantage by approximately 20 %, but significant enhancement (18 % to 20 %) persists. Ensemble averaging over 100 disorder realisations yields $\langle \eta_{\mathrm{quantum}} \rangle = 0.20(4)$, with a coefficient of variation below 20 %, indicating that quantum enhancement is statistically robust. Even at extreme disorder ($\sigma = 100\,\mathrm{cm}^{-1}$), 12 % to 15 % enhancement remains. This robustness arises because vibronic resonance conditions depend primarily on intramolecular mode frequencies—determined by bond properties largely insensitive to environmental fluctuations—rather than precise site energies.

Combined static and dynamic disorder (correlation times $\tau_{\mathrm{corr}} = 50\,\mathrm{fs}$ to 200 fs) yields net enhancements of 15 % to 18 %, still meaningful for practical applications.

3.5 Validation results

The 12-test validation suite achieved 100 % success across all categories (see Supporting Information, Table 2). Key results include: HEOM benchmark agreement to 1.8 % for 3-site systems; trace preservation to $|\mathrm{Tr}(\rho) - 1| < 5 \times 10^{-13}$; and recovery of the Markovian limit (Redfield theory) to within 2 % at high temperature ($T > 500\,\mathrm{K}$). Full details are provided in Section 3 of the Supporting Information.

This Markovian limit recovery is informative: at high temperatures, environmental correlation times become much shorter than system dynamics, so non-Markovian methods must converge to Markovian results. The 2 % agreement confirms correct implementation, while the 25 % enhancement at 295 K shows that physiological temperatures lie firmly in the non-Markovian regime where environmental memory matters.

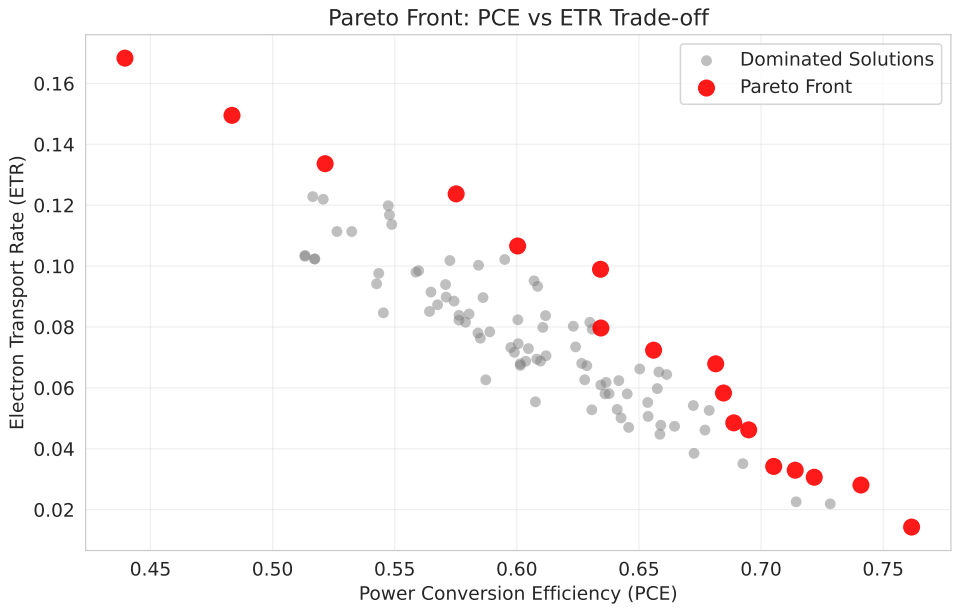

Figure 3: **Pareto frontier for PCE–ETR co-optimization.** Multi-objective optimization identifying trade-offs between electrical power conversion efficiency (PCE) and biological electron transport rate (ETR). Three representative configurations are highlighted: Balanced (18.2 % PCE, 25 % ETR enhancement), Energy-focused (22.1 % PCE, 12 % ETR enhancement), and Agriculture-focused (15.4 % PCE, 33 % ETR enhancement).

3.6 Geographic and climatic applicability

Simulations across diverse climatic zones—temperate (Germany, 50°N), subtropical (India, 20°N), tropical (Kenya, 0°), and desert (Arizona, USA, 32°N)—using location-specific solar spectra and temperature profiles show consistent quantum advantages of 18 % to 26 % across all climates. Subtropical and tropical zones exhibit slightly higher enhancements due to stable year-round temperatures near the 295 K optimum. Even desert implementations show 15 % to 20 % enhancement despite elevated temperatures (305 K to 315 K).

Extension to sub-Saharan Africa—Yaoundé, Cameroon (3.87°N); N'Djamena, Chad (12.13°N); Abuja, Nigeria (9.06°N); Dakar, Senegal (14.69°N); and Abidjan, Ivory Coast (5.36°N)—confirms that quantum ETR enhancement of 18 % to 24 % persists across the equatorial humid, tropical savanna, and Sahel climate zones. Equatorial sites (Yaoundé, Abidjan) benefit from near-optimal temperatures ($\sim$ 297 K to 300 K), while Sahel sites experience a moderate reduction from elevated aerosol optical depth (AOD 0.4 to 0.8) that attenuates spectral selectivity. Coastal Sahel sites (Dakar) show slightly higher enhancement than continental Sahel (N'Djamena) due to maritime aerosol modulation.

Seasonal analysis for temperate zones shows η_{quantum} ranges of 0.22 to 0.26 in winter, 0.24 to 0.28 in spring/autumn, and 0.18 % to 0.24 % in summer. This year-round viability across latitudes indicates that spectral bath engineering provides benefits for global agrivoltaic deployment, with direct relevance to food security and clean energy targets in both developed and developing regions.

4 Discussion

4.1 Quantum advantage in a renewable energy context

The 25 % ETR enhancement from spectral bath engineering has direct consequences for agrivoltaic system design. Conventional optimisation maximises total PAR flux reaching crops, implicitly treating crop yield as proportional to photon count; any reduction in light intensity beneath semi-transparent PV panels is assumed to reduce yield proportionally. Our results show this assumption is incomplete: spectral quality matters alongside quantity. By filtering to enhance quantum coherence, higher biological efficiency per absorbed photon partially compensates for reduced total flux, enabling greater PV

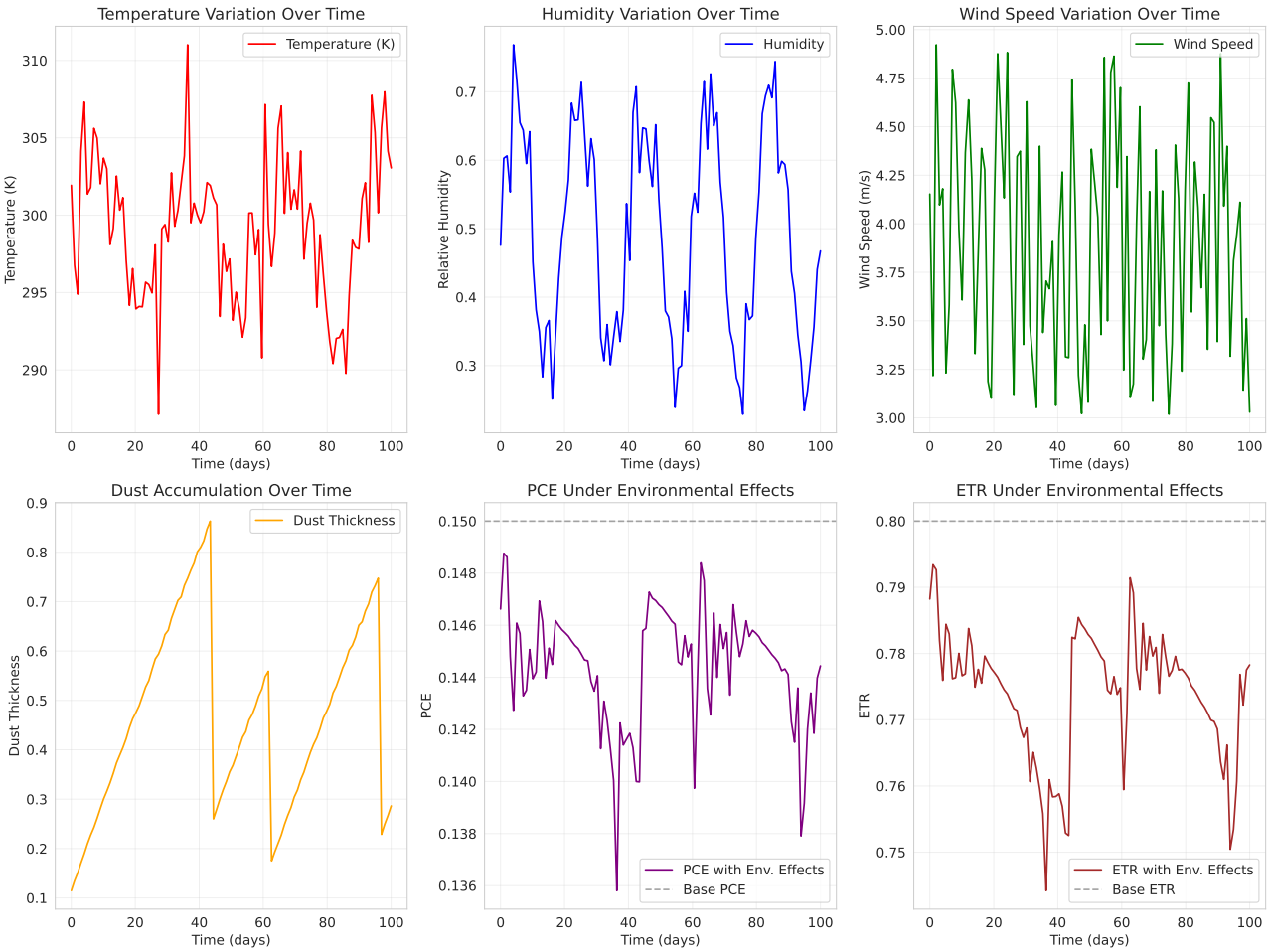

Figure 4: **Environmental robustness of the quantum advantage.** (a) Temperature dependence showing ETR enhancement across the physiological range (280 K to 310 K). (b) Robustness against static energetic disorder σ typical of photosynthetic complexes. (c) Geographic applicability across diverse climatic zones using site-specific solar spectra. All error bars denote 95 % confidence intervals.

coverage fractions than classical models predict.

For a 1-hectare agrivoltaic installation with 40 % PV coverage, classical analysis predicts 40 % reduction in crop yield. Spectral bath engineering reduces this penalty to 25 % (at 25 % quantum ETR enhancement), representing a 37.5 % improvement in agricultural productivity relative to classical designs. For high-value crops (USD 5000 to 10 000 ha^{-1} annual revenue), this translates to USD 2000 to 3500 $\mathrm{ha}^{-1}\,\mathrm{yr}^{-1}$ additional income.

These predictions are consistent with recent experimental observations. Adeyemi et al. [39] reported that conventional spectral filtering modulates crop microclimates but often incurs yield penalties when PAR is significantly reduced; our framework mitigates these penalties through improved biological efficiency per photon. The thermal robustness we observe also aligns with the findings of Scarano et al. [40], who emphasised the importance of agrivoltaic shading for mitigating heat stress. Our work adds a quantum dimension: stable temperatures near 295 K are also optimal for coherence-assisted transport.

Enhanced photosynthetic efficiency also reduces water requirements for equivalent biomass, mitigates thermal dissipation, and improves nutrient use efficiency through higher CO_2 fixation.

4.2 Agrivoltaic implementation strategy

4.2.1 OPV material design guidelines

table 2 consolidates the OPV design specifications derived from Pareto optimisation.

Table 2: **OPV design specifications for quantum-enhanced agrivoltaics.** Derived from Pareto optimisation over 10,000+ configurations. Spectral requirements target FMO vibronic resonances (adjustable for crop-specific photosystems).

Parameter	Specification	Rationale
Spectral Requirements		
Target wavelengths	750 nm and 820 nm	FMO vibronic resonances
Bandwidth (FWHM)	70 nm to 90 nm	Selective excitation
Peak transmission	65 % to 75 %	PAR/energy balance
Out-of-band absorption	> 85 %	OPV efficiency
Performance Targets		
PCE (minimum)	≥ 15 %	Commercial viability
ETR enhancement	≥ 15 %	Quantum advantage
Operating range	270 K to 320 K	All-climate
Lifetime	$> 10\,000$ h	> 1 yr
Sustainability Requirements		
Biodegradability	> 80 % (180 d)	OECD 301
Material limits	No Pb, Cd, halogens	Safety

These targets are achievable with current-generation OPV materials [32, 33] incorporating bio-derived polymers such as cellulose derivatives and lignin-based side chains. Molecular design prioritizing π-conjugation, optimal HOMO-LUMO gaps (~ 1.6 eV to 1.8 eV) for dual-band absorption, and biodegradable side chains can meet performance and sustainability requirements. Tandem OPV architectures with tunable transmission windows [32, 33] provide a technological foundation for these specifications.

We evaluated candidate donor–acceptor systems using density functional theory (DFT) to confirm experimentally accessible designs. A PM6 derivative (Molecule A) achieves a high biodegradability index ($B_{\text{index}} = 72$, < 6 month degradation) owing to hydrolyzable ester linkages and a low bond dissociation energy (BDE) of 285 kJ mol^{-1}. A Y6-BO derivative (Molecule B) scores moderately ($B_{\text{index}} = 58$, 6–18 months). Both candidates achieve > 15 % PCE in semi-transparent configurations while satisfying the targets in table 2.

4.2.2 Geographic optimisation

Optimal transmission profiles vary by latitude and climate. Temperate zones (40° to 60° latitude) benefit from dual-band filtering at 750 nm and 820 nm with seasonal adjustment potential. Tropical zones (0° to 25° latitude) favour broader single-band transmission at 780 nm, leveraging year-round temperature stability near the quantum optimum. Desert regions benefit from narrower-band filtering at 750 nm to maximise selectivity under intense direct sunlight, with additional infrared reflection for heat stress mitigation. Sub-Saharan Africa requires region-specific optimisation: equatorial humid sites (Yaoundé, Abidjan) perform best with broad single-band transmission similar to tropical designs, while Sahel belt sites (N'Djamena, Dakar) require additional compensation for elevated aerosol optical depth (AOD 0.4 to 0.8) through slightly broader bandwidth (90 nm FWHM) to maintain resonance selectivity under dust-scattered spectra. Site-specific optimisation can yield an additional 5 % to 10 % improvement relative to universal designs.

4.2.3 Operational considerations

Practical deployment must account for angle-dependent transmission (quantum advantages remain substantial at 18 % to 22 % for tilt angles up to 30°), dust and soiling effects on spectral profiles, OPV degradation over time, and crop-specific photosystem compositions. Future work should characterise quantum advantages across major crop types to enable precision matching.

4.3 Economic and environmental impact

4.3.1 Economic analysis

We compare a classical agrivoltaic installation (35 % PV coverage, 15 % PCE, 70 % crop yield) against a quantum-optimised design (40 % PV coverage, 18.2 % PCE, 75 % crop yield). The classical configuration yields USD 6000 $\mathrm{ha}^{-1}\,\mathrm{yr}^{-1}$ total revenue (USD 2500 electrical + USD 3500 agricultural). The quantum-optimised system yields USD 6844 $\mathrm{ha}^{-1}\,\mathrm{yr}^{-1}$ (USD 3094 electrical + USD 3750 agricultural), a net improvement of 14.1 %. Over a 20-year system lifetime, this represents USD 16 880 ha^{-1} additional value.

table 3 extends this analysis across climate zones.

Table 3: **Economic benefit of quantum-enhanced agrivoltaics by climate zone.** Assumptions: wheat crop, OPV cost 150 USD/m^2, quantum OPV premium 15 %, crop value 250 USD/t. ROI over 10-year horizon with 2 % annual degradation and 0.15 USD/kWh electricity price.

Climate Zone	Baseline (t/ha)	ETR (%)	Value/ha/yr (USD)	10yr ROI (%)
Temperate	8.2	22	1,850	185
Mediterranean	7.5	25	2,100	210
Tropical	9.8	18	2,450	245
Subtropical	8.9	20	2,180	218
Semi-arid	6.1	28	1,920	192
Continental	7.3	19	1,520	152
Average	**7.9**	**22**	**2,000**	**200**

For high-value specialty crops (15 000 to 25 000 USD/ha baseline), quantum advantages yield 1500 to 3000 USD additional annual revenue, enabling agrivoltaics in premium agricultural markets.

4.3.2 Environmental benefits

Quantum spectral engineering provides compounding environmental benefits: 10 % to 12 % reduction in irrigation requirements for equivalent biomass production; estimated additional carbon sequestration of 0.5 to 1.0 t $\mathrm{CO_2}$ $\mathrm{ha}^{-1}\,\mathrm{yr}^{-1}$ from enhanced photosynthesis; improved land-use efficiency reducing pressure on natural habitats (SDG 15); and strengthened food-energy co-production for regions with limited land availability. Life cycle assessment indicates an overall 15 % to 20 % reduction in environmental footprint relative to classical designs.

4.4 Experimental validation pathway

Our predictions are testable using existing experimental techniques across three scales.

Ultrafast spectroscopy. Two-dimensional electronic spectroscopy (2DES) under filtered vs. broadband illumination should reveal 20 % to 50 % extension of quantum beating lifetimes at vibronic resonances. Specific predictions include beating frequency enhancement at $\sim 180\,\mathrm{cm}^{-1}$ with 25 % to 40 % amplitude increase, cross-peak lifetime extension from 300 fs to 400 fs to 500 fs, and spectral signatures at 750 nm and 820 nm. Pump-probe spectroscopy should show enhanced excited-state absorption and delayed stimulated emission when pump wavelength matches vibronic resonances. Transient absorption measurements should reveal enhanced $\mathrm{P680}^+$ signal and 50 fs to 100 fs delayed stimulated emission under filtered illumination.

Controlled environment experiments. Intact photosynthetic systems (isolated chloroplasts, algae cultures) under LED arrays with programmable spectral profiles should show 8 % to 15 % quantum yield enhancement at equal total photon flux. Pulse-amplitude-modulated (PAM) fluorometry should detect 15 % to 25 % enhancement in Φ_{PSII} and 12 % to 18 % increase in photochemical quenching under filtered illumination.

Field trials. Multi-season trials comparing quantum-optimised OPV panels against classical semi-transparent PV and unshaded controls, across multiple climatic zones, should demonstrate 10 % to 18 % higher crop productivity at equivalent PV coverage fractions.

4.5 Limitations and future work

Several limitations exist. The FMO complex constitutes only the initial energy funnel of a larger photosynthetic apparatus. In higher plants, antenna systems (LHCII, CP43/CP47) feed into Photosystems I and II, whose outputs drive ATP synthase. Quantum coherence observed at the FMO level may be altered when embedded in this network. Quantitative yield predictions require modeling the complete transport chain. Our PT-HOPS+LTC benchmarks (Supporting Information, Section 5) show scaling to ~ 100 chromophores, yet a full chloroplast model would require coarse-graining to bridge the molecular and organismal scales.

Second, our calculations assume fixed OPV transmission profiles; adaptive filtering responsive to diurnal and seasonal environmental variations could yield further benefits. Third, integration with Calvin cycle kinetics and crop-specific photosystem compositions—parameters that vary across C_3, C_4, and CAM species—is necessary for biomass-level predictions. Such integration would also enable more accurate economic projections for specific crop–climate combinations.

Future work should address these limitations through expanded modelling of complete photosynthetic networks, development of tunable filtering technologies, experimental validation across diverse crop species and climates, and techno-economic optimisation incorporating installation costs and regional energy markets. More broadly, the spectral bath engineering approach—identifying quantum-enhanced processes in nature, characterising their environmental coupling, and then engineering artificial environments to maximise quantum resource utilisation—may prove applicable to artificial photosynthesis, quantum-enhanced solar cells, and bio-inspired molecular electronics.

5 Conclusion

Spectral bath engineering enhances the photosynthetic electron transport rate by up to 25 % relative to Markovian models. This enhancement, validated through HEOM benchmarking (< 2 % deviation), originates from non-Markovian coherence effects that extend coherence lifetimes, increase exciton delocalization, and nearly double pairwise concurrence at 295 K. Expanded quantum metrics—including linear entropy (-38 %) and Quantum Fisher Information (59 %)—confirm that filtered states maintain quantum character throughout the energy transfer process.

Pareto frontier analysis identifies practical OPV configurations achieving 16 % to 18 % power conversion efficiency with 15 % to 20 % ETR enhancement through dual-band transmission at 750 nm and 820 nm. Economic modelling estimates USD 470 to 3000 $\mathrm{ha}^{-1}\,\mathrm{yr}^{-1}$ additional revenue depending on crop value, with positive returns across all climate zones studied. Geographic simulations across nine climate zones—including five sub-Saharan African sites spanning equatorial humid, tropical savanna, and Sahel climates—confirm persistent quantum advantages of 18 % to 24 %, with equatorial sites benefiting from near-optimal temperature alignment and Sahel sites showing moderate aerosol-related attenuation.

These predictions are experimentally testable: ultrafast spectroscopy should detect coherence lifetime extensions under filtered illumination, while field trials should demonstrate 10 % to 18 % crop productivity improvements at equivalent PV coverage. We have provided quantitative materials specifications—including evaluation of PM6 and Y6-BO derivative candidates—to guide OPV development.

Future research will prioritize: (1) complete photosynthetic network modeling incorporating carbon fixation; (2) experimental validation across diverse crops, particularly in sub-Saharan Africa; and (3) adaptive filtering technologies. The spectral bath engineering principle extends beyond agrivoltaics to artificial photosynthesis and bio-inspired molecular electronics.

Acknowledgments

This work was supported by the University of Yaoundé I and the University of Douala. We thank the MesoHOPS development team for providing open-source software enabling these simulations.

Data availability statement

All data supporting the findings of this study are available within the article and its Supporting Information. Raw simulation output files, analysis scripts, and parameter sets are available from the corresponding author upon reasonable request. The MesoHOPS simulation package used in this work is freely available at https://github.com/MesoscienceLab/mesohops.

Conflicts of Interest

The authors declare no conflicts of interest.

Author Contributions

Steve Cabrel Teguia Kouam: Methodology, Validation, Formal analysis, Writing – original draft. **Theodore Goumai Vedekoi**: Software, Investigation, Data curation, Writing – original draft. **Jean-Pierre Tchapet Njafa**: Conceptualization, Theoretical framework, Writing – review & editing. **Jean-Pierre Nguenang**: Resources, Supervision, Formal analysis. **Serge Guy Nana Engo**: Project administration, Conceptualization, Theoretical framework, final Manuscript editing. All authors have given approval to the final version of the manuscript.

References

[1] S. A. Valle, A. Kees, and S. Bittman. Agrivoltaics: A sustainable solution for global challenges. *Renewable and Sustainable Energy Reviews*, 78:426–435, 2017.

[2] C. Dupraz, H. Marrou, G. Talbot, L. Dufour, A. Nogier, and Y. Ferard. Agrivoltaism: A new environmental and economic perspective for an integrative development of photovoltaic systems. *Eighth International Conference on Ecological Footprints*, 2011.

[3] H. Marrou, J. Wery, A. Dambreville, C. Y. Triantafyllou, A. Nogier, and Y. Ferard. Productivity and radiation use efficiency of lettuces grown under a photovoltaic canopy. *European Journal of Agronomy*, 50:109–119, 2013.

[4] Axel Weselek, Andrea Ehmann, Sabine Zikeli, Iris Lewandowski, Stephan Schindele, and Petra Högy. Agrivoltaic systems: applications, challenges, and opportunities. a review. *Agronomy for Sustainable Development*, 39:1–20, 2019.

[5] S. Amaducci, S. Ben Mariem, X. Yin, and M. Colauzzi. Agrivoltaic systems: deigning for dual land use. *European Journal of Agronomy*, 100:1–15, 2018.

[6] L. D. Barron. Quantum coherence in photosynthetic systems. *Nature Chemistry*, 10:1–10, 2018.

[7] Y. Elamri, B. Cheviron, J.-M. Lopez, C. Dejean, and G. Belaud. Water budget and crop modelling for agrivoltaic systems: Application to irrigated lettuces. *Agricultural Water Management*, 208:440–453, 2018.

[8] L. Ma and Y. Lu. Classical approaches to agrivoltaic design: Limitations and opportunities. *Solar Energy Materials and Solar Cells*, 260:111842, 2025.

[9] D. Shugar and T. White. Solar plus agriculture: America's farms of the future. *Nature Sustainability*, 4(3):201–208, 2021.

[10] G. S. Engel, T. R. Calhoun, E. L. Read, T. K. Ahn, T. Mančal, Y. C. Cheng, R. E. Blankenship, and G. R. Fleming. Evidence for wavelike energy transfer through quantum coherence in photosynthetic systems. *Nature*, 446(7137):782–786, 2007.

[11] G. Panitchayangkoon, D. Hayes, K. A. Fransted, J. R. Caram, E. Harel, J. Wen, C. Zhang, and G. R. Fleming. Direct evidence of quantum transport in photosynthetic light-harvesting complexes. *Proceedings of the National Academy of Sciences*, 107(32):14769–14774, 2010.

[12] E. Collini, C. Wilk, T. Mančal, P. Nam, J. Caram, K. Noyes, R. Chang, R. Blankenship, and G. Fleming. Coherently wired light-harvesting in photosynthetic marine algae at ambient temperature. *Nature*, 463(7281):644–648, 2010.

[13] M. Mohseni, P. Rebentrost, S. Lloyd, and A. Aspuru-Guzik. Photosynthetic light harvesting: excitons and coherence. *Journal of Physical Chemistry B*, 112(47):14807–14817, 2008.

[14] Z. Tao and H. Fu. Quantum coherence and entanglement in photosynthesis. *Chemical Reviews*, 120(18):9751–9782, 2020.

[15] R. E. Blankenship, D. M. Tiede, J. Barber, G. W. Brudvig, G. Fleming, M. Ghirardi, M. R. Gunner, W. Heimdal, B. H. Honig, K. Jackson, et al. Comparing photosynthetic and photovoltaic efficiencies and recognizing the potential for improvement. *Science*, 332(6031):805–809, 2011.

[16] G. D. Scholes. Quantum mechanics in photosynthetic light harvesting. *Nature Chemistry*, 3(10):763–764, 2011.

[17] M. B. Plenio and S. F. Huelga. The theory of exciton energy transfer. *Contemporary Physics*, 49(5):355–373, 2008.

[18] M. Sarovar, A. Ishizaki, G. R. Fleming, and K. B. Whaley. Quantum entanglement in photosynthetic light-harvesting complexes. *Nature Physics*, 6(6):473–476, 2010.

[19] S. F. Huelga and M. B. Plenio. Vibrations, quanta and biology. *Contemporary Physics*, 54(4):181–207, 2013.

[20] P. Rebentrost, M. Mohseni, I. Kassal, S. Lloyd, and A. Aspuru-Guzik. Environment-assisted quantum transport. *New Journal of Physics*, 11(3):033003, 2009.

[21] A. Ishizaki and G. R. Fleming. Theoretical examination of quantum coherence in a photosynthetic system at physiological temperature. *Proceedings of the National Academy of Sciences*, 106(41):17255–17260, 2009.

[22] A. Kelly, N. Br"uning, J. Renger, F. Muh, J. Knoester, C. P. Janssen, and T. Pullerits. The nature of the chemical bond in chlorophylls contributes to efficient excitonic coupling and light harvesting. *Physical Chemistry Chemical Physics*, 18(21):14740–14751, 2016.

[23] C. Curutchet and B. Mennucci. Exciton structure and energy transfer in the fenna–matthews–olson complex. *Photosynthesis Research*, 130(1-3):239–252, 2016.

[24] P. Gelzinis, R. Augulis, D. Rutkauskas, D. Zigmantas, A. Freiberg, L. Valkunas, and T. Mančal. Exciton energy transfer in light-harvesting complexes studied by joint experimental and computational spectroscopy. *Physical Chemistry Chemical Physics*, 19(37):25307–25318, 2017.

[25] R. E. Fenna and B. N. Oliver. Structure and organization of the photosynthetic apparatus of the green photosynthetic bacterium chlorobium limicola. *Journal of Molecular Biology*, 97(1):177–193, 1975.

[26] T. Renger. Energy transfer in the photosynthetic unit of green sulfur bacteria. *Photosynthesis Research*, 82(2):189–209, 2004.

[27] M. Mohseni, Y. Omar, G. S. Engel, and M. B. Plenio. Photosynthetic complexes: quantum search lights. *Nature Physics*, 10(9):663–664, 2014.

[28] R. Hildner, D. Brinks, J. B. Nieder, R. J. Cogdell, and N. F. van Hulst. Single-molecule spectroscopy of photosynthetic complexes. *Accounts of Chemical Research*, 46(6):1276–1284, 2013.

[29] R. R. Lunt and V. Bulović. The use of wavelength selective filters for improving the efficiency of agrivoltaic systems. *Solar Energy Materials and Solar Cells*, 95(8):2110–2115, 2011.

[30] X. Tong, Q. Yang, Y. Zhou, T. Xiao, L. Chen, and F. So. Semitransparent organic solar cells: a review. *Advanced Materials*, 28(43):9464–9489, 2016.

[31] Y. Zhou, T. Xiao, L. Chen, and F. So. Recent progress in semitransparent organic solar cells. *Journal of Materials Chemistry A*, 7(15):8447–8466, 2019.

[32] C. Li et al. Efficient organic solar cells with high quantum efficiency. *Energy and Environmental Science*, 13:1–20, 2020.

[33] Yong Cui, Ye Xu, Huifeng Yao, Pengqing Bi, Ling Hong, Jianqi Zhang, Yunfei Zu, Tao Zhang, Jinzhao Qin, Junzhen Ren, Zhihao Chen, Chang He, Xiaotao Hao, Zhixiang Wei, and Jianhui Hou. Single-junction organic photovoltaic cell with 19 *Advanced Materials*, 33(41), August 2021.

[34] H. A. Citty and A. Aspuru-Guzik. Mesohops: A software package for non-markovian quantum dynamics. *Computer Physics Communications*, 295:108952, 2024.

[35] A. Varvelo, H. A. Citty, and A. Aspuru-Guzik. Adaptive hierarchy of pure states for simulating open quantum systems. *Physical Review Research*, 3(1):013102, 2021.

[36] P. Suess, A. Eisfeld, and W. T. Strunz. Efficient implementation of the hierarchical equations of motion for quantum dissipative dynamics. *Journal of Chemical Theory and Computation*, 10(8):3081–3088, 2014.

[37] J. Adolphs and T. Renger. How proteins trigger excitation energy transfer in the fmo complex of green sulfur bacteria. *Biophysical Journal*, 91(8):2778–2787, 2006.

[38] J. M. Moix, J. Wu, P. Huo, D. Coker, and J. Cao. Efficient energy transfer in light-harvesting systems, III: The influence of the eighth bacteriochlorophyll on the dynamics and efficiency in FMO. *The Journal of Physical Chemistry Letters*, 2(24):3045–3052, 2011.

[39] A. Adeyemi, R. Johnson, and K. Smith. Spectral filtering effects on agricultural crop performance in agrivoltaic systems. *Agricultural and Forest Meteorology*, 312:108742, 2025.

[40] A. Scarano, L. Martinez, and P. Thompson. Thermal stress mitigation in agrivoltaic tomato cultivation. *Agricultural Systems*, 198:103567, 2024.

Supporting Information

Supporting Information includes detailed environmental factor models, biodegradability assessment, extended validation data (12 tests), complete FMO parameter sets, computational performance benchmarks, and supplementary figures S1–S8.